Wake-body Resonance of Long Flexible Structures is Dominated by Counterclockwise Orbits

Wake-body Resonance of Long Flexible Structures is Dominated by Counterclockwise Orbits

Rémi Bourguet,[1,*] Yahya Modarres-Sadeghi,[2] George E. Karniadakis,[3] and Michael S. Triantafyllou[1]

[1]*Massachusetts Institute of Technology, Cambridge, Massachusetts 02139, USA*
[2]*University of Massachusetts, Amherst, Massachusetts 01003, USA*
[3]*Brown University, Providence, Rhode Island 02912, USA*

(Received 7 June 2011; published 23 September 2011)

We identify a dominant mechanism in the interaction between a slender flexible structure undergoing free vibrations in sheared cross-flow and the vortices forming in its wake: energy is transferred from the fluid to the body under a resonance condition, defined as wake-body frequency synchronization close to a natural frequency of the structure; this condition occurs within a well-defined region of the span, which is dominated by counterclockwise, figure-eight orbits. Clockwise orbits are associated with damping fluid forces.

DOI: 10.1103/PhysRevLett.107.134502 PACS numbers: 47.32.ck, 47.27.ek, 47.54.De

Introduction.—A bluff body, i.e., an object with a blunt cross section as opposed to a streamlined object, immersed in cross-flow forms a wake which is unstable, resulting in the formation of large-scale vortical structures that induce unsteady forces on the body. If the body is flexible or flexibly mounted, vortex-induced vibrations (VIV) result, which can have significant implications for a number of physical systems, from aeolian harps to cables and risers placed in ocean currents. The VIV phenomenon has been a major object of research throughout the years [1–3]. In this Letter, we clarify the mechanisms of vortex-induced excitation of a long flexible structure within a sheared cross-flow, when energy is exchanged between the fluid and the body, but is also redistributed along the length of the structure, resulting in complex interactions.

A flexibly mounted rigid cylinder placed within a current and free to oscillate in the cross-flow (CF) direction, viz., the direction perpendicular to the oncoming flow, has become the canonical problem in fluid-structure interaction. Work by several investigators has helped elucidate the fundamentals of VIV [1–8]. Large amplitude oscillations occur when the frequency of vortex formation is relatively close to a natural frequency of the structure; then the frequency of vortex shedding can be entrained and become equal to the frequency of the structural CF vibration; this wake-body resonance condition is referred to as *lock-in*. A notable feature under the resonance condition is that the vibration frequency can shift from the natural frequency [2]. Substantial differences exist when the rigid cylinder is also allowed to move in the inline (IL) direction, the direction parallel to the oncoming flow [9,10]. Inclusion of the IL motion leads to significant changes in hydrodynamic forces acting on the rigid cylinder, depending on the phase difference between the IL and the CF vibrations [11,12].

The case of a long flexible cylinder within a cross-flow is very important for applications; yet it has received far less attention, because of the complexities associated with the distributed interaction between the fluid and the flexible body, including the difficulty to pinpoint the region where the fluid excites the body, and identifying the mechanisms of energy redistribution along the span.

Detailed laboratory experiments on flexible structures placed in cross-flow have provided information on the amplitude of vibration, excited frequencies and structural wave numbers [13]. For long flexible cylinders, contrary to the case of rigid cylinders, the phase difference between the IL and CF displacements can vary along the span, leading to diverse trajectories along the structure. On the basis of structure response measurements, [14,15] have hypothesized a possible link between the orientation of the IL/CF cylinder trajectory and the excitation or damping of the structure vibrations by the flow. However, it is still unclear whether a relation can be established between the occurrence of the lock-in condition, the fluid-structure energy transfer and the orientation of the cylinder trajectory. We address this question in the present Letter by means of a joint analysis of the structure response and wake pattern, based on detailed numerical simulation and experimental results.

Simulation and experiment.—For both the numerical simulation and the experiment a tensioned beam is employed with a circular cross section, pinned at both ends and free to move in the IL (x) and CF (y) directions. The beam is subject to an oncoming flow parallel to the x axis and linearly sheared along the z axis [Fig. 1(a)]. As shown in the following, the sheared flow velocity profile allows to identify regions of lock-in and regions of non-lock-in along the span. The beam length (L) to diameter (D) ratio is equal to 200 in the simulation and 1400 in the experiment [13]. In the simulation, the ratio between the maximum and minimum inflow velocities is equal to 3.67. In the experiment, inflow velocity is zero at $z = L$. The Reynolds number based on D and the maximum inflow velocity, which occurs at $z = 0$, is equal to 330 in the simulation and 19 000 in the experiment. The small structure-to-fluid

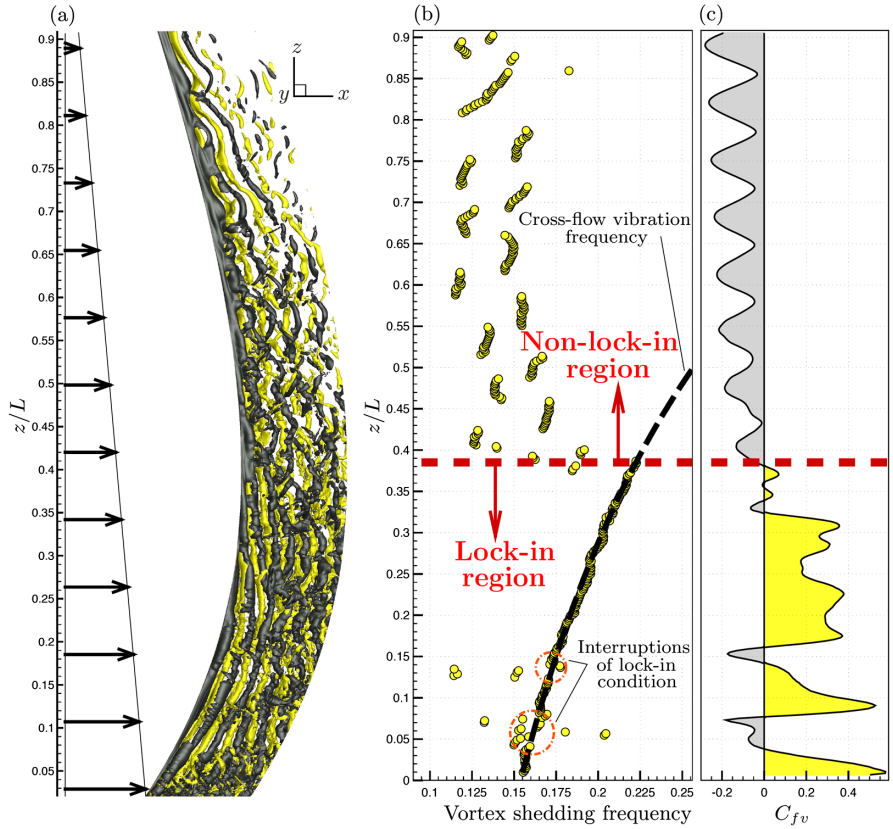

FIG. 1 (color online). (a) Instantaneous isosurfaces of the spanwise vorticity nondimensionalized by the cylinder diameter and the maximum inflow velocity, $\omega_z = \pm 0.3$; only part of the computational domain is plotted: [0.6D, 25D] downstream of the cylinder. (b) Spanwise evolution of the vortex shedding frequency; the cylinder CF vibration frequency is indicated by a black dashed line. The CF vibration frequency and the corresponding natural frequency differ by 0.5%. (c) Fluid-structure energy transfer: spanwise evolution of the time-averaged fluid force coefficient in phase with the cylinder velocity (C_{fv}); excitation (damping) in yellow (gray).

mass ratio (≤ 3 in both cases) and the selected tension and bending stiffness which lead to vibrations involving high structural wave numbers, are representative of configurations encountered in the field.

Direct numerical simulation of the incompressible Navier-Stokes equations based on the spectral hp element method [16] is used to predict the three-dimensional flow past the tensioned beam [17]. The experimental data are from the Norwegian Deepwater Programme (NDP) [13]. The time series of structure displacements are determined from acceleration measurements at eight points along the span. Both numerical and experimental time series correspond to more than 40 CF oscillation cycles.

Results.—The IL and CF structure vibrations consist of a mixture of standing and traveling wave patterns [17]. Maximum vibration amplitudes of 0.8D–0.9D are reached in the CF direction and 0.2D–0.3D in the IL direction. The spanwise evolution of the vibration frequencies shows that the IL response occurs at twice the frequency of the CF vibration, as also observed in previous work. As expected for mixed cable-beam structures, the excited structural wave number in the IL direction is not necessarily equal to twice the CF one, because the relation between a spatial wave number and the corresponding natural frequency is not linear, and the fluid force in phase with the structure acceleration is not the same in the two directions [18].

Based on the numerical study, the wake is principally composed of obliquely shed vortex rows, often interconnected through vortex splitting events, similar to those observed in rigid cylinders [19] [Fig. 1(a)]. In Fig. 1(b), the vortex shedding frequency is plotted along the span together with the cylinder CF vibration frequency. The frequencies are nondimensionalized by D and the local oncoming flow velocity. The lock-in condition, i.e., the local synchronization of the vortex shedding and CF vibration frequencies, occurs over a large spanwise region located on the high-velocity side; this zone is referred to as lock-in region. Under lock-in, the vortex shedding frequency is driven far from the Strouhal frequency observed in the case of a stationary cylinder; here, lock-in occurs in the frequency range 0.155–0.22. The limit of the lock-in region is indicated by a red dashed line in Fig. 1(b). Beyond the lock-in region the vortex shedding frequency is different from the vibration frequency and exhibits a discontinuous, cellular pattern. The fluid force coefficient in phase with the cylinder velocity, including both the IL

and CF directions and averaged over the entire time series (C_{fv}), is used to quantify the energy transfer between the flow and the vibrating cylinder [12]. A positive C_{fv} implies a transfer of energy from the fluid to the structure, and therefore flow-induced excitation. The spanwise evolution of C_{fv} [Fig. 1(c)] shows that the structure is excited by the flow ($C_{fv} > 0$) in the lock-in region and damped by the flow ($C_{fv} < 0$) in the non-lock-in region.

The IL and CF vibration frequencies have a ratio of 2, leading to "figure-eight" trajectories in the (x, y) plane. The instantaneous phases of the IL and CF vibrations, ϕ_x and ϕ_y, respectively, are determined by means of the Hilbert transform. The phase difference between the IL and CF displacements is $\Phi_{xy} = [p\phi_x - q\phi_y, \mod 360°]$, where $p = 1$ and $q = 2$, since the synchronization is studied for a frequency ratio of 2 [20]. Phase difference values in the range 0°–180° correspond to trajectories where the cylinder moves upstream when reaching the CF oscillation maxima ("counterclockwise", CC) and phase difference values in the range 180°–360° correspond to trajectories in the opposite direction ("clockwise", C) [11]. The histograms of Φ_{xy} evaluated from the simulation time series are plotted in Fig. 2(a), along the span. The transition from CC to C trajectories ($\Phi_{xy} = 180°$) is indicated by a vertical black line and the limit of the lock-in region, as identified previously, by a horizontal red dashed line. At each spanwise location, a preferential phase difference and thus a specific trajectory can be clearly identified. For $z/L < 0.16$, approximately, both the IL and CF vibrations exhibit pronounced standing wave patterns. As a

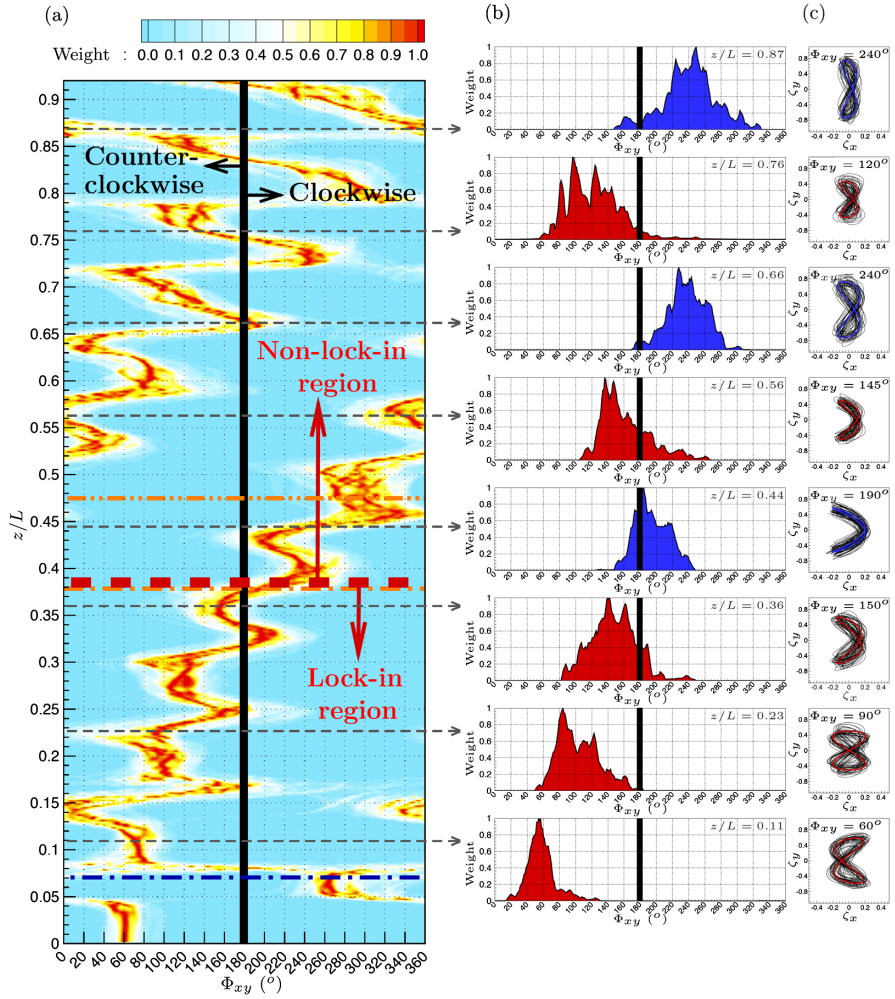

FIG. 2 (color online). Spanwise evolution of the histogram of phase difference between the IL and CF displacements (Φ_{xy}): (a) numerical simulation, (b) experiment. In (a), the limit of lock-in region is indicated by a red dashed line (simulation); for the experiment, the estimated upper limits are indicated by orange dashed-dotted and dashed-double-dotted lines, lower limit by a blue dashed-dotted line. Locations of measurement points in (b) are indicated by gray dashed arrows in (a). (c) CF (ζ_y) versus IL (ζ_x) displacements nondimensionalized by the cylinder diameter (black line) and characteristic orbits (colored line), same location points as in (b) (experiment). In (b) and (c), histograms and characteristic orbits are colored according to the preferential orientation: CC (C) in red (blue).

consequence, switchings between the CC and C trajectories are observed near the nodes of the IL displacement at $z/L \approx 0.04$, $z/L \approx 0.08$, and, to a lesser extent, at $z/L \approx 0.12$ and $z/L \approx 0.16$. Beyond this region, the switching CC-C pattern is altered by the development of mainly traveling waves oriented from high to low velocity regions (increasing z), still modulated by an underlying standing wave component. The fact that the nodes of standing wave pattern in the CF direction do not necessarily correspond to the IL displacement nodes further perturbs the above alternating pattern. Pure traveling waves in both directions could lead to constant Φ_{xy} along the span [14], while pure standing waves with a ratio of 2 between the IL and CF excited structural wave numbers would be associated with a switching CC-C pattern, as observed near $z = 0$. In the present case of mixed standing-traveling wave responses, Φ_{xy} exhibits a zigzagging spanwise pattern, drifting toward higher phase difference angles as z increases. The CC trajectories are predominant in the lock-in region. In addition, the short spanwise interruptions of the lock-in condition at $z/L \in [0.04, 0.08]$ and around $z/L \approx 0.14$ [areas shown in Fig. 1(b)], which are associated with a strong decrease and even a negative peak of C_{fv} (the latter resulting, on average, in vibration damping), coincide with occurrence of C trajectories.

In the experimental results, location of the lock-in region can be estimated by considering a synchronization window of $\pm 20\%$ about a reduced flow velocity of 5.9 [21] leading to a frequency range of 0.14–0.21. The lower and upper limits of the estimated lock-in region are indicated in Fig. 2(a) by blue and orange dashed-dotted lines. Another estimate proposed by [15] for the NDP experiments, leads to a frequency range of 0.1–0.25 and the lock-in region upper limit indicated by an orange dashed-double-dotted line. This lock-in region reaches $z = 0$, as in the simulation. The histograms of Φ_{xy} based on the experimental time series are shown in Fig. 2(b). The corresponding cylinder trajectories are plotted in Fig. 2(c) (black lines), as well as selected characteristic orbits (colored lines). Regardless of the estimation used for the lock-in bandwidth, the cylinder exhibits mainly CC trajectories in the lock-in region. This is observed for all the cases in the NDP experiments, as long as a frequency ratio of 2 can be identified between the IL and CF displacements.

Discussion and conclusion.—Despite differences in the physical parameters (body aspect ratio, shear rate, Reynolds number), both numerical simulation and experimental results highlight the existence of a predominant orbit orientation in the lock-in region. For an elastically mounted rigid cylinder in uniform flow, [11] noted that the CC trajectories lead to a closer proximity of the cylinder and the recently shed vortices and to a specific phasing between cylinder motion and vortex forces leading to stable resonant vibrations; also the shed vorticity is stronger due to the upstream motion of the cylinder at the extremes of the trajectory [11]. The persistence of CC orbits within the region of lock-in confirms that similar mechanisms are employed in the case of flexible cylinders.

In summary, we find that the vortex-induced vibrations of long flexible bodies are excited by positive energy transfer within a lock-in region, characterized by counterclockwise orbits; hence in-line and cross-flow vibrations are locked to a specific phase difference range. The clockwise orbits primarily occur outside the lock-in region and are principally associated with damping fluid forces.

*bourguet@mit.edu

[1] T. Sarpkaya, J. Fluids Struct. **19**, 389 (2004).
[2] C. H. K. Williamson and R. Govardhan, Annu. Rev. Fluid Mech. **36**, 413 (2004).
[3] P. W. Bearman, J. Fluids Struct. **27**, 648 (2011).
[4] P. W. Bearman, Annu. Rev. Fluid Mech. **16**, 195 (1984).
[5] A. Ongoren and D. Rockwell, J. Fluid Mech. **191**, 197 (2006).
[6] J. Carberry, J. Sheridan, and D. Rockwell, J. Fluid Mech. **538**, 31 (2005).
[7] J. S. Leontini, B. E. Stewart, M. C. Thompson, and K. Hourigan, Phys. Fluids **18**, 067101 (2006).
[8] T. K. Prasanth and S. Mittal, J. Fluid Mech. **594**, 463 (2007).
[9] D. Jeon and M. Gharib, J. Fluids Struct. **15**, 533 (2001).
[10] N. Jauvtis and C. H. K. Williamson, J. Fluid Mech. **509**, 23 (2004).
[11] J. M. Dahl, F. S. Hover, M. S. Triantafyllou, S. Dong, and G. E. Karniadakis, Phys. Rev. Lett. **99**, 144503 (2007).
[12] J. M. Dahl, F. S. Hover, M. S. Triantafyllou, and O. H. Oakley, J. Fluid Mech. **643**, 395 (2010).
[13] A. D. Trim, H. Braaten, H. Lie, and M. A. Tognarelli, J. Fluids Struct. **21**, 335 (2005).
[14] J. K. Vandiver, V. Jaiswal, and V. Jhingran, J. Fluids Struct. **25**, 641 (2009).
[15] Y. Modarres-Sadeghi, H. Mukundan, J. M. Dahl, F. S. Hover, and M. S. Triantafyllou, J. Sound Vib. **329**, 43 (2010).
[16] G. E. Karniadakis and S. Sherwin, *Spectral/hp Element Methods for CFD* (Oxford Univ. Press, Oxford, 1999).
[17] R. Bourguet, G. E. Karniadakis, and M. S. Triantafyllou, J. Fluid Mech. **677**, 342 (2011).
[18] R. Bourguet, G. E. Karniadakis, and M. S. Triantafyllou, J. Fluids Struct. **27**, 838 (2011).
[19] C. H. K. Williamson, J. Fluid Mech. **243**, 393 (2006).
[20] F. J. Huera-Huarte and P. W. Bearman, J. Fluids Struct. **25**, 969 (2009).
[21] J. K. Vandiver, J. Fluids Struct. **7**, 423 (1993).